



Influence of spark plasma sintering on microstructure and wear behaviour of Ti–6Al–4V reinforced with nanosized TiN

Oluwasegun Eso FALODUN¹, Babatunde Abiodun OBADELE¹, Samuel Ranti OKE¹, Oladeji Oluremi IGE¹, Peter Apata OLUBAMBI¹, Moipone Linda LETHABANE², Shepherd Willie BHERO³

1. Centre for Nanoengineering and Tribocorrosion, School of Mining, Metallurgy and Chemical Engineering, University of Johannesburg, South Africa;

2. Department of Chemical, Metallurgical and Materials Engineering, Tshwane University of Technology, Pretoria, South Africa;

3. Department of Engineering Metallurgy, University of Johannesburg, Doornfontein Campus, Doornfontein, Johannesburg, South Africa

Received 14 November 2016; accepted 23 January 2017

Abstract: Ti–6Al–4V/TiN composites were successfully consolidated by spark plasma sintering (SPS). TiN addition to Ti–6Al–4V was varied from 1% to 5% (volume fraction). The effect of TiN addition on the densification, microstructure, microhardness and wear behaviour of Ti–6Al–4V was studied. Experimental results showed reduction in sintered density of the compacts from 99% to 97% with increase in TiN content. However, an increase in microhardness value was recorded from HV_{0.1} 389 to HV_{0.1} 488. X-ray diffraction (XRD) analysis showed that the intensity of diffraction peaks of TiN phase in the composites increased also with formation of small amount of secondary Ti₂N phase. SEM analysis of SPS sintered nanocomposites possessed a refinement of α/β phase microstructure in Ti–6Al–4V with the presence of uniformly dispersed TiN particles. The worn surface of the composite showed improved abrasive wear resistance with non-continuous grooves as compared to the sintered Ti–6Al–4V without TiN addition.

Key words: spark plasma sintering; Ti–6Al–4V; TiN; microstructure; wear

1 Introduction

Design and processing of new materials for high temperature applications has maintained a challenge in many engineering fields. New engineering materials are required in such harsh environments and this has been an emerging research all over the world [1]. The primary attributes of Ti and Ti alloys make them very popular as competitive metal matrix materials and lauded as a strong alternative to traditional metals for a number of other reasons, for example, their high specific strength allows them to fulfill the increasing demand for engineering materials with light weight, high strength in turbine engines, airframes and automotive industries [2,3]. Ti–6Al–4V is the most widely used of all $\alpha+\beta$ Ti alloys with aluminum as α phase stabilizer and vanadium as β phase stabilizer [4,5]. However, Ti alloys have been limited due to the loss in mechanical strength

at high temperature (Ti alloys strength deteriorates as the temperature rises thereby limiting their use to approximately 400 °C) and inferior wear resistance. These disadvantages have limited the usage of Ti alloys in structural and industrial applications [6]. It has been reported that Ti alloys are rarely used where wear resistance is required due to poor fretting fatigue resistance and poor tribological properties [7,8]. These limitations provide scientific and technological interest for researchers to develop titanium matrix composites with improved mechanical and wear properties.

Superior properties of metal matrix composites (MMCs) such as wear resistance, mechanical strength and fracture toughness compared to the monolithic counterparts are due to the effect of reinforcement phases [9]. Reinforcing Ti alloys with hard precipitates such as titanium nitride (TiN), helps with the improvement of corrosion and wear resistance of the materials, with unique properties such as high hardness,

high chemical and physical stability, good thermal and electrical conductivity, high melting point, good resistance to wear and corrosion, excellent biocompatibility and excellent performance as an adhesion layer. Spark-plasma-sintering of nanostructured TiN powder was performed by GROZA et al [10]. Studies of conventional sintering of nanocrystalline TiN powders were undertaken by RABE and WÄSCHE [11] and CASTRO and YING [12]. To the best of the authors' knowledge, fabrications of TiN reinforced Ti–6Al–4V alloys through spark plasma sintering are rarely discussed in the available literature.

Spark plasma sintering is a synthesis and processing technique used to rapidly sinter powder materials at high temperatures within a short period of time as compared to conventional sintering such as hot pressing, pressureless sintering and hot isostatic pressing which required longer sintering period.

This work focuses on improving the mechanical and wear properties of Ti–6Al–4V alloy with TiN addition using spark plasma sintering. The microstructural evolution and wear performance are discussed.

2 Experimental

The Ti based composites were developed using commercially pure Ti–6Al–4V powder (average particle size of 25 μm and purity of 99.9%, supplied by TLS-Technik, Germany) and TiN (average particle size of 20 nm and purity of 97%, supplied by Nanostructured & Amorphous Material Inc., Texas, USA). Varying compositions of TiN (1, 2, 3, 4 and 5, volume fraction, %) were added to Ti–6Al–4V and blended in a Turbula shaker mixer for 6 h in order to achieve homogenous mixture of the powders. Thereafter, the admixed powders were consolidated using spark plasma sintering equipment (HHPD–25 FCT type SPS equipment, Germany) in an argon atmosphere. Prior to the SPS process, the admixed powders were loaded into a graphite die with internal diameter of 40 mm and

thickness of 5 mm. The sintering temperature was firstly optimized from 800 to 1000 $^{\circ}\text{C}$ (see Table 1) in order to obtain maximum relative density of about 99%. Thereafter, the sintering temperature was set to be 1000 $^{\circ}\text{C}$ at a constant heating rate of 100 $^{\circ}\text{C}/\text{min}$, applied pressure of 50 MPa and holding time of 10 min. The sintered samples were then sandblasted to remove any surface graphite contamination.

The microstructure of the synthesized composites was evaluated using field emission scanning electronic microscope (JEOL JSM–7600F) equipped with energy dispersive X-ray spectroscopy (EDS) at an accelerating voltage of 15 kV. An X-ray diffraction (PW1710 Philips diffractometer, with monochromatic Cu K radiation at 40 kV and 20 mA) was performed to identify the presence of the constituent phases of the sintered composites. A search-match of the phases was done using an Highscore X'Pert Software. Densification of the sintered samples was carried out using Archimedes method while the theoretical density of the composite was calculated in accordance to the rule of mixture.

Microindentation test was done by using a Vickers microhardness tester (FUTURE-TECH FM 800) at room temperature upon a polished surface at a load of 0.98 N and dwell time of 15 s. The wear studies were carried out using a CETR UMT–2 tribometer (now Bruker) with a rotary wear module. A tungsten carbide (WC) ball with 10 mm in diameter was used as a counterface rubbing against the composites. Different loads of 5, 15 and 25 N were applied at a frequency of 1 Hz corresponding to 60 r/min at ambient temperature. The coefficient of friction (COF) and wear depth were monitored continuously during the test.

3 Results and discussion

3.1 As-received powder characterization

The as-received Ti–6Al–4V and TiN powders were characterized using SEM and EDS. Figures 1(a, b) show the typical SEM morphologies of the as-received

Table 1 Result of SPS optimization at different sintering temperature, density and microhardness of Ti–6Al–4V/TiN composites

Sample	Sintering temperature/ $^{\circ}\text{C}$	Relative density/%	Effective density/ $(\text{g}\cdot\text{cm}^{-3})$	Microhardness ($\text{HV}_{0.1}$)
Ti–6Al–4V	800	97.29	4.31	358
Ti–6Al–4V	900	98.64	4.37	374
Ti–6Al–4V	1000	99.54	4.41	389
Ti–6Al–4V+1%TiN	1000	99.32	4.41	417
Ti–6Al–4V+2%TiN	1000	98.87	4.39	438
Ti–6Al–4V+3%TiN	1000	98.42	4.38	451
Ti–6Al–4V+4%TiN	1000	97.53	4.35	475
Ti–6Al–4V+5%TiN	1000	97.08	4.33	488

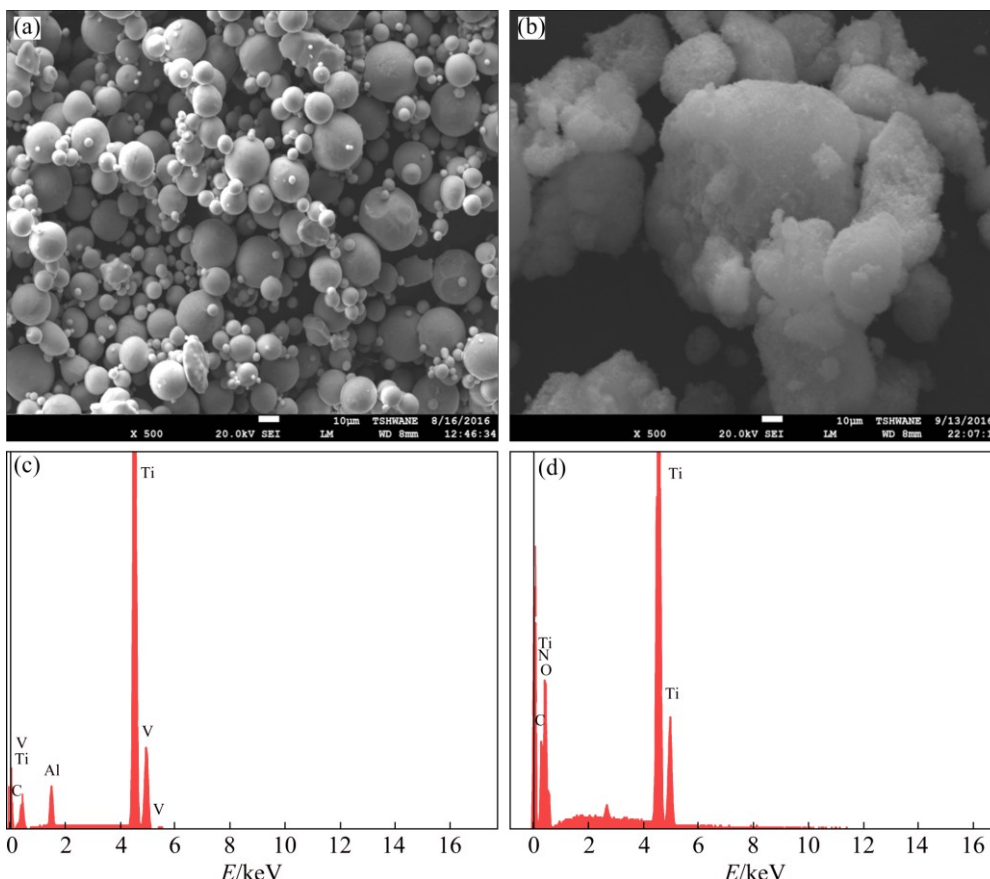


Fig. 1 SEM morphologies and EDS spectra of as-received Ti-6Al-4V (a, c) and TiN powders (b, d)

powders. The Ti-6Al-4V particles (Fig. 1(a)) are spherical and non-porous with several agglomerated satellites that stick to the larger particles. The presence of satellites indicates that the Ti-6Al-4V was produced through gas atomization [13,14]. Figure 1(b) shows that the TiN particles are spherical and lumpy. EDS analysis (Figs. 1(c, d)) confirms that Ti-6Al-4V contains Ti, Al and V while TiN powder consists of Ti, N and O.

3.2 Relative density

Figure 2 shows the relative densities of Ti-6Al-4V alloy without and with addition of TiN as a function of sintering temperature and volume fraction. From Fig. 2(a), it is obvious that the relative density of sintered Ti-6Al-4V alloy increased from 97.29% to 99.54% with increasing sintering temperature from 800 °C to 1000 °C. This suggests that relative density of 99% could only be attained by SPS when Ti-6Al-4V is sintered at 1000 °C, where full densification was achieved. GARBIEC et al [15] reported that during spark plasma sintering of Ti-6Al-4V, an effective relative density of 99.54% was achieved at sintering temperature of 1000 °C and compaction pressure of 50 MPa. Likewise, TEBER et al [16] confirmed that an increase in density is as a result of decrease in the level of porosities as well as increase in temperature. However, at constant sintering

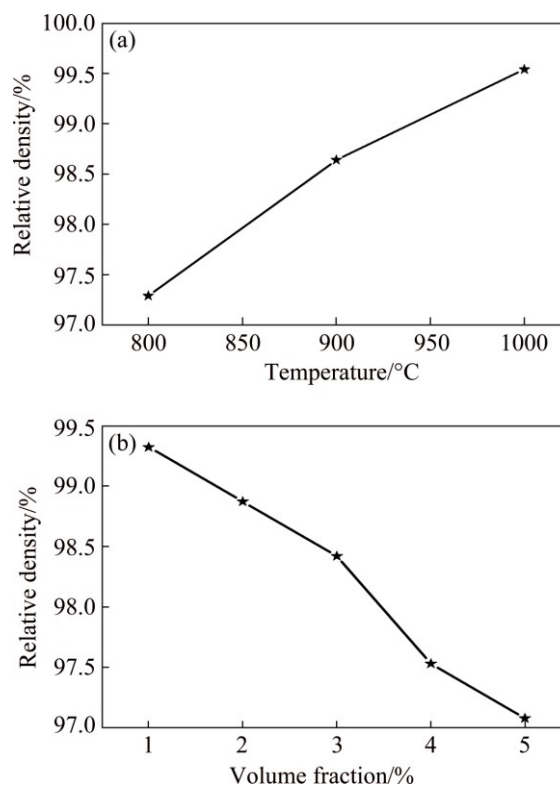


Fig. 2 Relative density of sintered compacts of Ti-6Al-4V: (a) At different sintering temperatures; (b) With TiN addition at different volume fractions

temperature of 1000 °C for sintered compacts of Ti-6Al-4V/TiN, it was observed that the relative density decreased from 99% to 97% when TiN is increased from 1% to 5% (volume fraction). The addition of TiN could result in the presence of residual pores within the matrix. BHAUMIK et al [17] also confirmed that the introduction of TiN resulted in a high sintered porosity.

3.3 XRD analysis and microstructural characteristics

The XRD patterns of consolidated Ti-6Al-4V/TiN compacts at sintering temperature of 1000 °C are illustrated in Fig. 3. The XRD spectra confirm the presence of both α -Ti and β -Ti phases while high intensities of diffraction peaks corresponding to the TiN phase are detected in the composites. The increase in intensity of TiN with increasing concentration in Ti-6Al-4V matrix was also reported by BALLA et al [9]. All the sintered Ti-6Al-4V compacts with TiN addition revealed the existence of intermediate phase, such as Ti₂N. Sintering at high temperature causes significant nitrogen diffusion and thus leads to phase transformation of TiN to Ti₂N.

SEM micrographs of Ti-6Al-4V without and with addition of TiN sintered at 1000 °C are shown in Fig. 4.

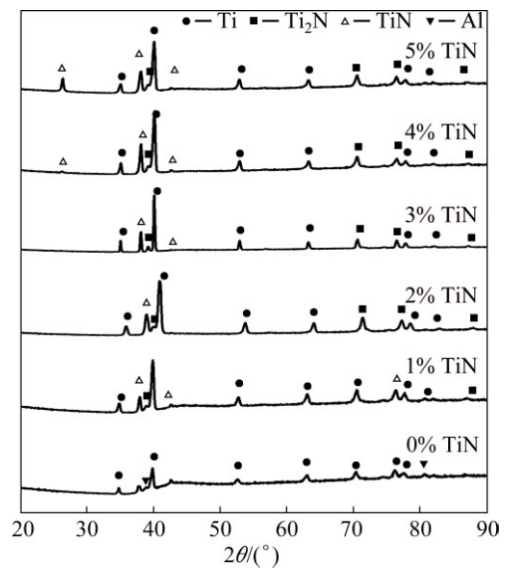


Fig. 3 XRD patterns for sintered Ti-6Al-4V with varying volume fraction of TiN

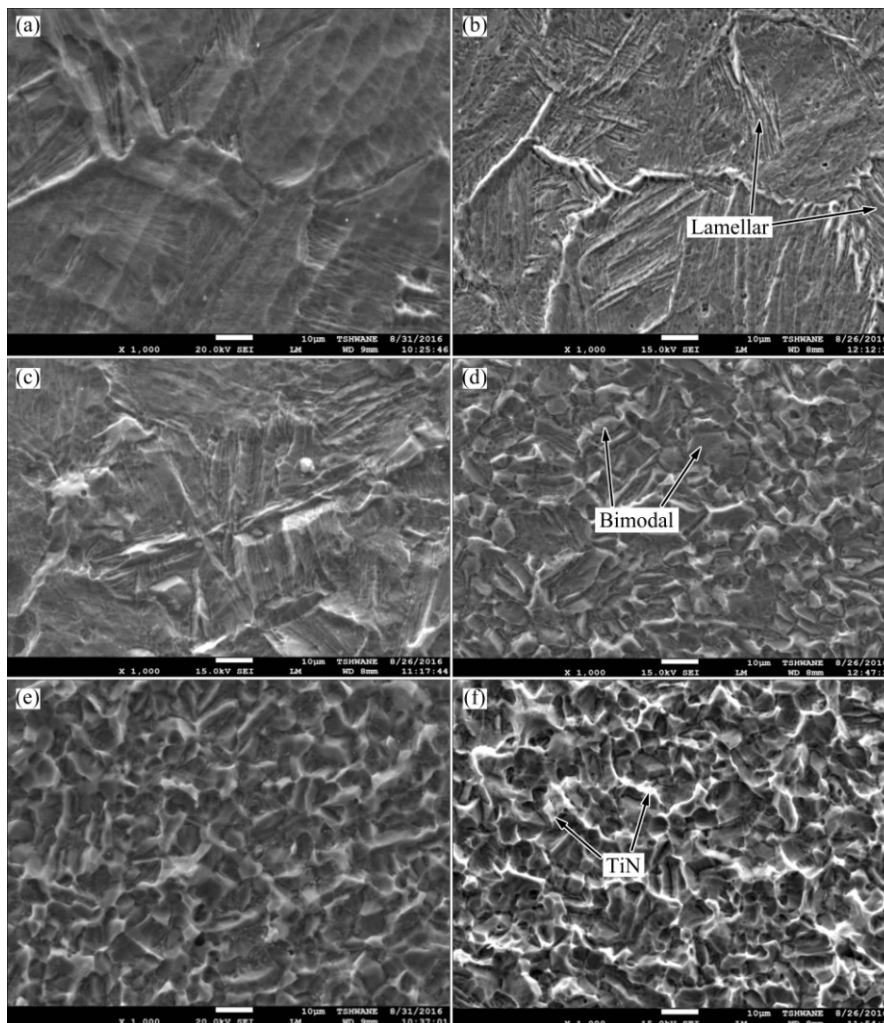


Fig. 4 Scanning electron micrographs of sintered samples: (a) Ti-6Al-4V; (b) Ti-6Al-4V-1TiN; (c) Ti-6Al-4V-2TiN; (d) Ti-6Al-4V-3TiN; (e) Ti-6Al-4V-4TiN; (f) Ti-6Al-4V-5TiN

Typical microstructure of sintered Ti-6Al-4V alloy is presented in Fig. 4(a) which comprises a non-porous microstructure with two distinct phases [18,19]. The presence of aluminium and vanadium helps to stabilize α and β phase, respectively [20,21]. The microstructures of Ti-6Al-4V/TiN composites are shown in Figs. 4(b–f) which are different from the microstructure observed in Fig. 4(a). In the composites with 1%–2% TiN, as shown in Figs. 4(b) and (c), it is obvious that a lamellar α/β structure was formed. However, it is noted that micrographs with 3%–5% TiN revealed a significance microstructural difference as compared with 1%–2% TiN and no interfacial porosity was observed throughout the composite. In other words, the microstructure was changed from lamellar to bimodal structure after the addition of 3%–5% TiN. This could be as a result of α stabilization from nitrogen present in TiN. The nano-scale size ranges of the TiN powder make it possible to fill potential pore spaces within the mixed powders and are seen along the grain boundaries of the structures. These microstructural observations indicate an interaction between TiN particles and Ti-6Al-4V alloy during spark plasma sintering processing.

3.4 Microhardness

Figure 5 illustrates the hardness of the sintered composites with different volume fractions of TiN. It is observed that the addition of nitride influences and enhances the hardness of the sintered composites. The hardness value of the Ti-6Al-4V was $HV_{0.1}$ 389 while microhardness value with addition of 1%–5% TiN ranges from $HV_{0.1}$ 417 to $HV_{0.1}$ 488. With the increase of TiN content, the increasing trend of the hardness is very evident when TiN content is less than 5%. The microstructure contribution to the observed increase in hardness was as a result of uniform distribution of TiN particles and Ti_2N hard phases in Ti-6Al-4V matrix.

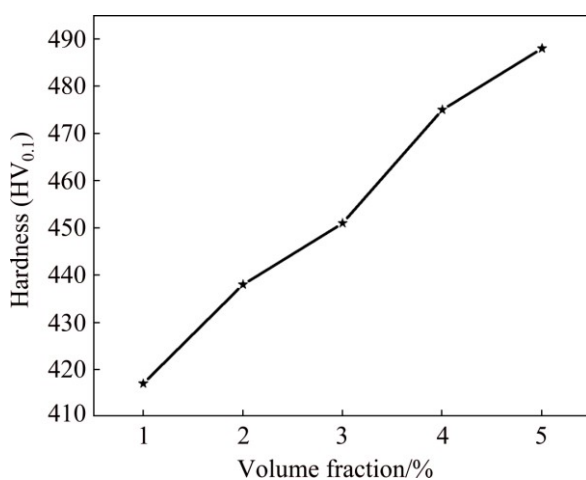


Fig. 5 Hardness variation with TiN content for Ti-6Al-4V based composites

3.5 Wear study

3.5.1 Wear behaviour

Figure 6 shows the observed variation of friction coefficient with rotary time at different loads of 5, 15 and 25 N. As shown in Figs. 6(a–c), the recorded steady-state friction coefficients for all the samples range from 0.3 to 0.5 irrespective of the applied load. The fluctuation behavior of the friction coefficient of Ti-6Al-4V with and without TiN is similar when the load was increased from 5 to 25 N. Wear debris generated as a result of relative movement of the counterface ball on the

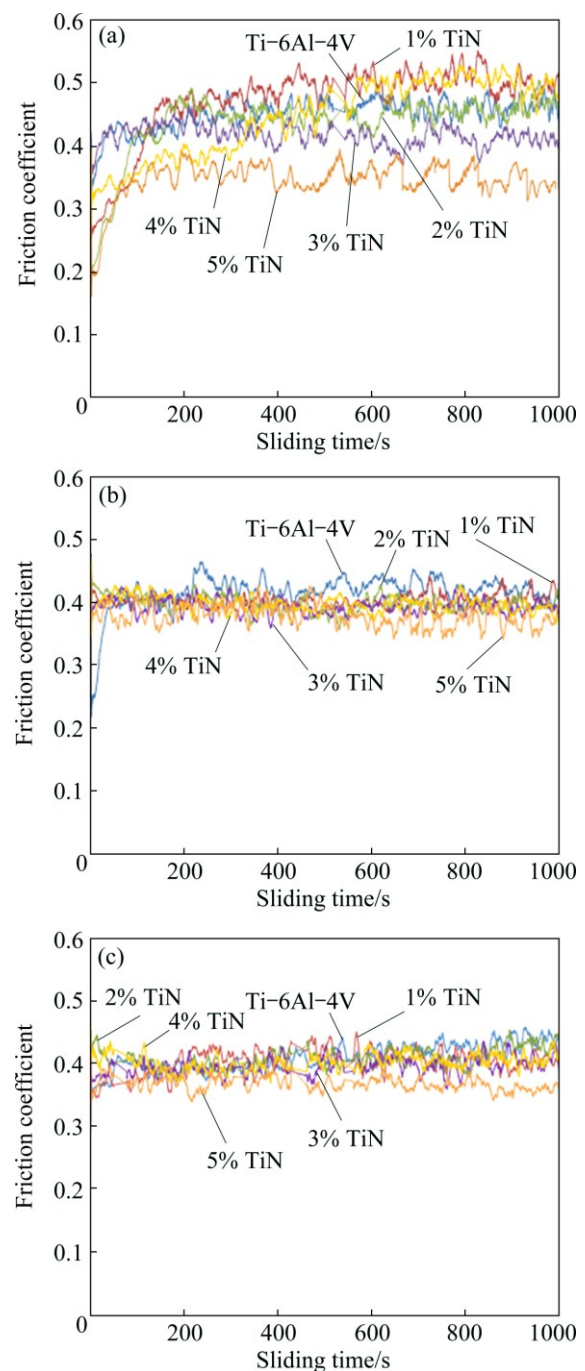


Fig. 6 Variation of friction coefficients of Ti-6Al-4V with and without TiN under different applied loads: (a) 5 N; (b) 15 N; (c) 25 N

compacts under higher loads could also influence the values of friction coefficient recorded. It could be noted that while most of the debris are ejected from the worn surface, the rest could be present as plateau on the wear track with high content of metal oxides, thereby providing lubricating effect, thus low friction coefficient. In all, the least friction coefficient was recorded with 5% TiN addition. This indicates that increasing TiN content could result in increasing size and distribution of TiN phase in the matrix thereby improving the wear resistance significantly [22]. The results obtained typically agree with reported work [9], which indicated that TiN reinforced Ti-6Al-4V alloy composite coatings have higher potential wear resistance compared with Ti-6Al-4V without TiN. Thus, it gives evidence that the addition of nano-TiN can protect the Ti-6Al-4V material under dry wear conditions to a great extent [23].

3.5.2 Worn surface morphology under rotary condition

Figure 7 indicates the SEM images of the worn

surface on Ti-6Al-4V alloy and composites with addition of TiN under applied load of 25 N. From Fig. 7(a), it could be seen that sintered Ti-6Al-4V alloy shows severe adhesive wear, abrasive wear and aggressive ploughing which resulted in deep grooves. This could be attributed to low microhardness value of Ti-6Al-4V and as a result poor abrasive resistance. MOLINARI et al [24] indicated that the poor wear resistance of Ti-6Al-4V is as a result of low plastic shearing resistance and low protection by the surface oxide as a result of high flash temperature generated by friction. As reported by FU et al [22], the high chemical response and high ductility of Ti-6Al-4V alloy could lead to its strong tendency for adhesion which could become work-hardened in the worn area and thus resulted in deep abrasive groves as shown in Fig. 7(a).

Figures 7(b–f) show the worn surface of Ti-6Al-4V-TiN (1%, 2%, 3%, 4% and 5%, volume fraction) sliding against WC ball under 25 N normal load. Unlike

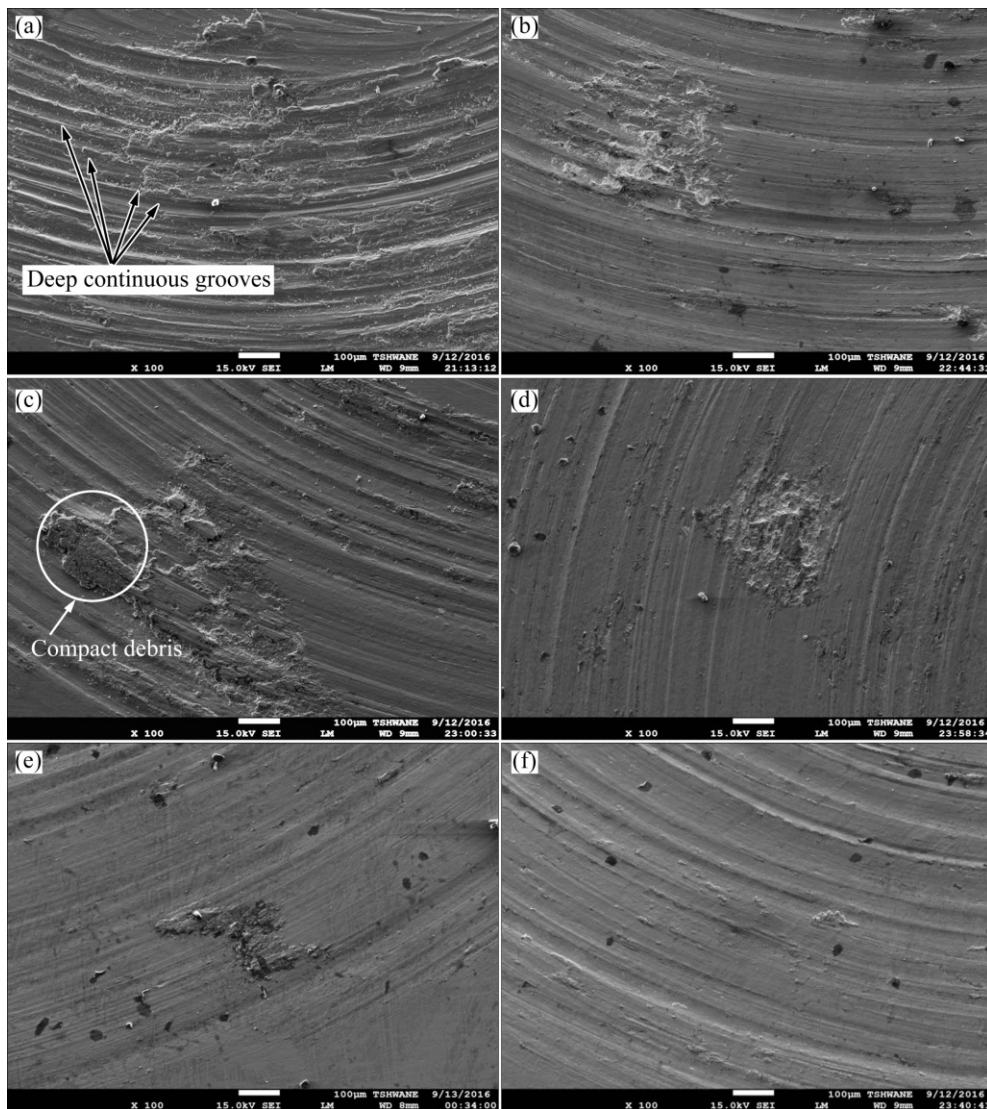


Fig. 7 SEM images of worn surface: (a) Ti-6Al-4V; (b) Ti-6Al-4V-1TiN; (c) Ti-6Al-4V-2TiN; (d) Ti-6Al-4V-3TiN; (e) Ti-6Al-4V-4TiN; (f) Ti-6Al-4V-5TiN

Ti–6Al–4V, the wear scar on the compacts surface is fairly smooth (shallow grooves) with no microfracture and cracks. This indicates that abrasive wear level decreases with increasing TiN addition to Ti–6Al–4V. This observation was also reported by CUI et al [25], FU et al [22] and GUO et al [26], and was attributed to the presence of hard phase (TiN). However, slight adhesive wear is noticeable on the wear surface of the composites. Generally, increasing TiN phase in Ti–6Al–4V leads to higher hardness and more resistance to wear. So, the wear resistance of Ti–6Al–4V+5%TiN was higher than that of Ti–6Al–4V under the same wear test conditions, as shown in Figs. 7(a) and (f).

4 Conclusions

1) The relative density of the Ti–6Al–4V+5%TiN composites decreased with the increasing of TiN volume fraction.

2) The addition of TiN showed a change in the microstructure from lamellar α/β structure to a bimodal structure. TiN particles were detected along the grain boundaries of the structures and distributed uniformly in the matrix, which exhibited good interface bonding between reinforcement and the matrix alloy.

3) Ti–6Al–4V+5%TiN had higher microhardness value than sintered Ti–6Al–4V alloy due to the presence of homogenous distribution of TiN particles and Ti₂N phases. An increase in hardness was recorded as the volume fraction of TiN increased from 1% to 5%.

4) The resistant to abrasive and adhesive wear increased with increasing TiN content and this was evident from the wear grooves produced on the worn surface.

References

- [1] FARAG M M. Quantitative methods of materials substitution: Application to automotive components [J]. *Materials & Design*, 2008, 29: 374–380.
- [2] XUE F, JIEHE S, YAN F, WEI C. Preparation and elevated temperature compressive properties of multi-walled carbon nanotube reinforced Ti composites [J]. *Materials Science and Engineering A*, 2010, 527: 1586–1589.
- [3] KONDOH K, THRERUJIRAPAPONG T, UMEDA J, FUGETSU B. High-temperature properties of extruded titanium composites fabricated from carbon nanotubes coated titanium powder by spark plasma sintering and hot extrusion [J]. *Composites Science and Technology*, 2012, 72: 1291–1297.
- [4] LÜTJERING G, WILLIAMS J C. *Titanium based intermetallics* [M]. Berlin: Springer, 2007.
- [5] OBADELE B A, ANDREWS A, OLUBAMBI P A, MATHEW M T, PITYANA S. Effect of ZrO₂ addition on the dry sliding wear behavior of laser clad Ti6Al4V alloy [J]. *Wear*, 2015, 328–329: 295–300.
- [6] LONG Y, GUO W J, LI Y. Bimodal-grained Ti fabricated by high-energy ball milling and spark plasma sintering [J]. *Transactions of Nonferrous Metals Society of China*, 2016, 26: 1170–1175.
- [7] VLCAK P, CERNY F, DRAHOKOUPIL J, SEPITKA J, TOLDE Z. The microstructure and surface hardness of Ti6Al4V alloy implanted with nitrogen ions at an elevated temperature [J]. *Journal of Alloys and Compounds*, 2015, 620: 48–54.
- [8] HAO Y, LIU J, LI J, LI S, ZOU Q, CHEN X. Rapid preparation of TiC reinforced Ti6Al4V based composites by carburizing method through spark plasma sintering technique [J]. *Materials & Design*, 2015, 65: 94–97.
- [9] BALLA V K, BHAT A, BOSE S, BANDYOPADHYAY A. Laser processed TiN reinforced Ti6Al4V composite coatings [J]. *Journal of the Mechanical Behavior of Biomedical Materials*, 2015, 6: 9–20.
- [10] GROZA J R, CURTIS J D, KRÄMER M. Field-assisted sintering of nanocrystalline titanium nitride [J]. *Journal of the American Ceramic Society*, 2000, 83: 1281–1283.
- [11] RABE T, WÄSCHE R. Sintering behaviour of nanocrystalline titanium nitride powders [J]. *Nanostructured Materials*, 1995, 6: 357–360.
- [12] CASTRO D T, YING J Y. Synthesis and sintering of nanocrystalline titanium nitride [J]. *Nanostructured Materials*, 1997, 9: 67–70.
- [13] ÖZBILEN S. Satellite formation mechanism in gas atomised powders [J]. *Powder Metallurgy*, 1999, 42: 70–78.
- [14] RAO G A, SRINIVAS M, SARMA D S. Effect of oxygen content of powder on microstructure and mechanical properties of hot isostatically pressed superalloy Inconel 718 [J]. *Materials Science and Engineering A*, 2006, 435–436: 84–99.
- [15] GARBIEC D, SIWAK P, MRÓZ A. Effect of compaction pressure and heating rate on microstructure and mechanical properties of spark plasma sintered Ti6Al4V alloy [J]. *Archives of Civil and Mechanical Engineering*, 2016, 16: 702–707.
- [16] TEBER A, SCHOENSTEIN F, TÊTARD F, ABDELLAOUI M, JOUINI N. Effect of SPS process sintering on the microstructure and mechanical properties of nanocrystalline TiC for tools application [J]. *International Journal of Refractory Metals and Hard Materials*, 2012, 30: 64–70.
- [17] BHAUMIK S K, UPADHYAYA G S, VAIDYA M L. Effect of TiN addition on sintering behaviour and mechanical properties of WC-10Co hard metals containing Mo₂C and Ni [J]. *Journal of Materials Science*, 1992, 27: 1947–1959.
- [18] da SILVA L, UEDA M, SILVA M, CODARO E. Corrosion behavior of Ti–6Al–4V alloy treated by plasma immersion ion implantation process [J]. *Surface and Coatings Technology*, 2007, 201: 8136–8139.
- [19] DUAN H Q, HAN Y F, LÜ W J, MAO J W, WANG L Q, ZHANG D. Effect of solid carburization on surface microstructure and hardness of Ti–6Al–4V alloy and (TiB+La₂O₃)/Ti–6Al–4V composite [J]. *Transactions of Nonferrous Metals Society of China*, 2016, 26: 1871–1877.
- [20] BRUNETTE D M, TENGVALL P, TEXTOR M, THOMSEN P. *Titanium in medicine: Material science, surface science, engineering, biological responses and medical applications* [M]. 2nd ed. Berlin: Springer, 2012.
- [21] OBADELE B A, ANDREWS A, MATHEW M T, OLUBAMBI P A, PITYANA S. Improving the tribocorrosion resistance of Ti6Al4V surface by laser surface cladding with TiNiZrO₂ composite coating [J]. *Applied Surface Science*, 2015, 345: 99–108.
- [22] FU Y, ZHANG X C, SUI J F, TU S T, XUAN F Z, WANG Z D. Microstructure and wear resistance of one-step in-situ synthesized TiN/Al composite coatings on Ti6Al4V alloy by a laser nitriding process [J]. *Optics & Laser Technology*, 2015, 67: 78–85.
- [23] YANG Z L, OUYANG J H, LIU Z G, LIANG X S. Wear mechanisms of TiN–TiB₂ ceramic in sliding against alumina from room temperature to 700 °C [J]. *Ceramics International*, 2010, 36: 2129–2135.

- [24] MOLINARI A, STRAFFELINI G, TESI B, BACCI T. Dry sliding wear mechanisms of the Ti6Al4V alloy [J]. *Wear*, 1997, 208: 105–112.
- [25] CUI Z D, ZHU S L, MAN H C, YANG X J. Microstructure and wear performance of gradient Ti/TiN metal matrix composite coating synthesized using a gas nitriding technology [J]. *Surface and Coatings Technology*, 2005, 190: 309–313.
- [26] GUO B, ZHOU J, ZHANG S, ZHOU H, PU Y, CHEN J. Microstructure and tribological properties of in situ synthesized TiN/Ti₃Al intermetallic matrix composite coatings on titanium by laser cladding and laser nitriding [J]. *Materials Science and Engineering A*, 2008, 480: 404–410.

放电等离子烧结对纳米 TiN 增强 Ti-6Al-4V 显微组织和磨损行为的影响

Oluwasegun Eso FALODUN¹, Babatunde Abiodun OBADELE¹, Samuel Ranti OKE¹, Oladeji IGE¹, Peter Apata OLUBAMBI¹, Moipone Linda LETHABANE², Shepherd Willie BHERO³

1. Centre for Nanoengineering and Tribocorrosion, School of Mining, Metallurgy and Chemical Engineering, University of Johannesburg, South Africa;
2. Department of Chemical, Metallurgical and Materials Engineering, Tshwane University of Technology, Pretoria, South Africa;
3. Department of Engineering Metallurgy, University of Johannesburg, Doornfontein Campus, Doornfontein, Johannesburg, South Africa

摘要: 采用放电等离子烧结(SPS)成功制备 Ti-6Al-4V/TiN 复合材料。加入 Ti-6Al-4V 中的 TiN 含量变化范围为 1%~5%(体积分数)。研究添加 TiN 对 Ti-6Al-4V 材料致密度、显微组织、硬度和磨损行为的影响。实验结果表明,随着 TiN 含量的增加,材料的烧结密度从 99%降低至 97%;而显微硬度值却从 HV_{0.1} 389 增加至 HV_{0.1} 488。X 射线衍射(XRD)分析表明,伴随着少量二次 Ti₂N 相的形成,复合材料中 TiN 相的衍射峰强度增加。SEM 分析表明,SPS 烧结 Ti-6Al-4V 纳米复合材料具有细化的 α/β 相组织及均匀分散的 TiN 颗粒。与无添加烧结 Ti-6Al-4V 相比, Ti-6Al-4V/TiN 复合材料的磨损表面呈现非连续的凹槽,抗磨粒磨损性能得到提高。

关键词: 放电等离子烧结; Ti-6Al-4V; TiN; 显微组织; 磨损

(Edited by Bing YANG)